

Random Persistence Diagram Generation

Farzana Nasrin *

Theodore Papamarkou †

Vasileios Maroulas ‡

Abstract

Topological data analysis (TDA) studies the shape patterns of data. Persistent homology (PH) is a widely used method in TDA that summarizes homological features of data at multiple scales and stores this in persistence diagrams (PDs). As TDA is commonly used in the analysis of high dimensional data sets, a sufficiently large amount of PDs that allow performing statistical analysis is typically unavailable or requires inordinate computational resources. In this paper, we propose random persistence diagram generation (RPDG), a method that generates a sequence of random PDs from the ones produced by the data. RPDG is underpinned (i) by a parametric model based on pairwise interacting point processes for inference of persistence diagrams and (ii) by a reversible jump Markov chain Monte Carlo (RJ-MCMC) algorithm for generating samples of PDs. The parametric model combines a Dirichlet partition to capture spatial homogeneity of the location of points in a PD and a step function to capture the pairwise interaction between them. The RJ-MCMC algorithm incorporates trans-dimensional addition and removal of points and same-dimensional relocation of points across samples of PDs. The efficacy of RPDG is demonstrated via an example and a detailed comparison with other existing methods is presented.

Keywords Dirichlet tessellation, interacting point processes, Markov chain Monte Carlo (MCMC), persistent homology, reversible jump MCMC, and confidence intervals.

1 Introduction

Persistent homology (PH) is a TDA tool that provides a robust way to probe information about the shape of datasets and to summarize salient features PDs. These diagrams are multisets of points in the plane, each point representing a homological feature whose time of appearance and disappearance is contained in the coordinates of that point [1]. Intuitively, the homological features represented in a PD measure the connectedness of data as their resolution changes. PH has proven to be promising in a variety of applications such as shape analysis [2], image analysis [3,4], neuroscience [5–7], dynamical systems [8], signal analysis [9], chemistry and material science [10,11], and genetics [12].

*Department of Mathematics, University of Hawaii at Manoa, Honolulu, HI (fnasrin@hawaii.edu)

†Department of Mathematics, The University of Manchester

‡Department of Mathematics, University of Tennessee, Knoxville, TN

There have been a number of notable contributions to develop statistical methods for performing inference on topological summaries. Many of these methods introduce probability measures for PDs to capture statistical information such as means, variance, and conditional probabilities [13–15]. Kernel densities are used by [16] to estimate the persistence diagrams generated by point process samples drawn by a particular distribution. [7] constructs a kernel density estimator built with machinery from finite set statistics for nonparametric estimation of persistence diagram probability densities.

Hypothesis testing and determining confidence sets for persistence diagrams are discussed in [17–21]. One of the main motivations to establish statistical methods for hypothesis testing and estimating confidence sets for PH is to distinguish topologically significant features from noise features. [18] develops a probability distribution of persistent homological invariant constructed from subsamples of a fixed size addresses the problem of statistical inference through a variety of test statistics obtained from a pertinent empirical distribution. [17] analyze a statistical model for persistence diagrams obtained from the level set filtration of the density estimator depending on the bottleneck stability theorem. All of these approaches either rely on a nonparametric permutation test or reduce persistence diagrams to a summary statistic and make use of bootstrapping.

Subsampling either the dataset or their PDs to compute statistics of the subsamples, to estimate confidence sets of persistence diagrams is proposed in [21]. The authors of [21] provide a bound on the bottleneck distance by means of Hausdorff distance and in turn derive the confidence set for PDs. Another article that thoroughly explores the limiting theorems and confidence sets for PD is [22]. Distance functions based on distance-to-measure (DTM) and kernel density estimation (KDE) are considered, and the limiting theorem of the empirical DTM depending on the quantile function of the push forward probability is derived. As opposed to the work of [21], the algorithm proposed by [22] finds different confidence bands for different homological features. The work in [23] develops a parametric approach based on a Gibbs measure that takes the interaction between points in a PD into consideration and offers a simulation of persistence diagrams through MCMC sampling [23,24]. The MCMC sampling method of these studies relies on an assumption of fixed number of points per PD sample.

We are specifically interested in defining an appropriate parametric model by viewing PDs as spatially inhomogeneous pairwise interacting point processes. Typically the majority of the points in a PD are located near the birth axis. The upper portion which usually consists of fewer points captures topological information about the data. To this end, we rely on a spatially inhomogeneous model to treat stochastically the location of points in PDs. Furthermore, the persistence coordinates of points in a PD indicate the prominence level of corresponding topological features. For example, typically points with brief persistence may result from noise whereas, longer persistence points represent important topological features. Furthermore, the pairwise distance between points in a PD contains information about the underlying data set. Nearby points usually share similar topological features and points that are further away mostly represent contrasting features. A step interaction function with parameters depending on the pairwise distance between points in a PD is capable of extracting the level of similarity in the corresponding topological features and consequently becomes an appropriate choice of interaction function.

Our work proposes a computational device based on maximum pseudolikelihood for estimating the model parameters. In particular, we combine the quadrature method referred as Berman-Turner device [25] with Dirichlet tessellation to get the maximum pseudolikelihood estimators. There are two important attributes of using Dirichlet tessellation: (i) it assigns higher weights to points that do not have nearby points; (ii) the quadrature method augments the number of points in a PD by dummy points and allows us to perform statistical inference even with a limited number of points in the PD. Typically in a PD the topologically significant points stay in the upper portion of the graph, fewer in number, and are separated from each other. So, the former attribute proves to be useful as it assigns higher weights to these significant points. Finally, we develop the *first* RJ-MCMC based sampling method to generate random persistence diagrams. This method allows three types of actions namely addition, removal, and relocation of points. Due to allowing addition and removal of points, the sampling process becomes trans-dimensional, therefore a RJ-MCMC is developed. The amplified space of PD points of our RJ-MCMC sampler traverses the state spaces of PDs more effectively (see Section 4). The sampling technique provides a theoretical setting for many statistical inferences. For example, (i) hypothesis testing to distinguish topological signals from noise, (ii) sensitivity and correlation analysis of the underlying point process model, and (iii) computational Bayesian inference.

To summarize, the main contributions of this work are:

1. A novel parametric model to capture the spatial structure of persistence diagrams.
2. A quadrature based pseudolikelihood maximization approach for estimating model parameters.
3. The *first* reversible jump MCMC algorithm that generates random PDs and is flexible enough to accommodate the randomness in the location of points and number of points.

This paper is organized as follows. Section 2 provides a brief overview of PDs and pairwise interacting point processes (PIPP). In Section 3, we present the methodology of RPDG. Precisely, in Section 3.1, we establish the parametric model to characterize PDs by integrating Dirichlet partition and PIPPs. Estimation of the parameters in this model is presented in Section 3.2. In Section 3.3, we provide the RJ-MCMC algorithm to generate random samples of PDs. RPDG is demonstrated and compared to alternative methods in section 4. We state our conclusion in Section 5. Finally, we present the proof of the proposition 3.1 and the justification of our model design in the appendix.

2 Preliminaries

We begin by discussing the necessary background for generating the parametric model for PDs. Section 2.1 briefly reviews the construction of PDs. Basic definitions and facts about PIPPs are discussed in Section 2.2.

2.1 Persistence Diagrams

Definition 2.1. Let $X = \{x_1, \dots, x_n\}$ be a point cloud in \mathbb{R}^d . The Vietoris-Rips complex $\text{VR}(\epsilon)$ of X is defined to be the simplicial complex $V_\epsilon(X)$ satisfying $[x_{i_1}, \dots, x_{i_l}] \in V_\epsilon(X)$ if and only if $\text{diam}(x_{i_1}, \dots, x_{i_l}) < \epsilon$. Given a nondecreasing sequence $\{\epsilon_n\} \in \mathbb{R}^+ \cup \{0\}$ with $\epsilon_0 = 0$, we denote its Vietoris-Rips filtration by $\{V_{\epsilon_n}(X)\}_{n \in \mathbb{N}}$.

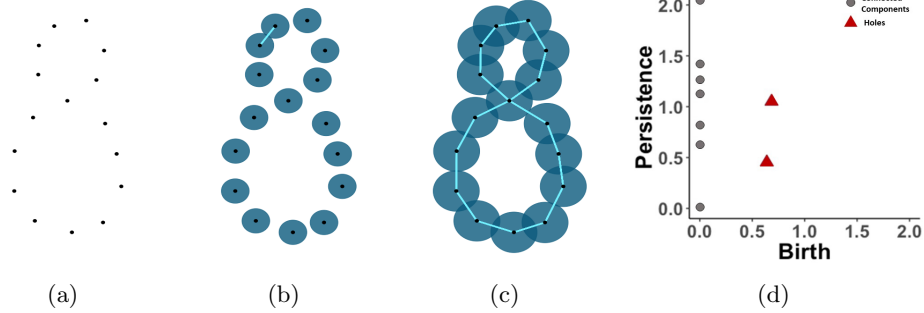


FIG. 1: (a) An underlying dataset of points. (b) The Vietoris-Rips complex consists of the points and the light blue line segment. (c) The Vietoris-Rips complex with a larger ϵ than (b) consists of points and line segments that now form an “eight” shape, which has two 1-dimensional holes. (d) The tilted PD for connected components and holes associated with the Vietoris-Rips complex in (c).

Formally, for each homological dimension, a PD is a multiset of points (b, d) , where b is the radius in the Vietoris-Rips complex at which a homological feature is born and d is the radius at which it dies. Intuitively, the homological features represented in a PD are connected components or holes of different dimensions. To illustrate the Vietoris-Rips complexes we present a toy example in Fig. 1 by considering an “eight” shape in (a). The algorithm starts by taking into account circles with increasing radii (at each algorithmic step) centered at each data point. As the “resolution” of the data changes, homological features emerge or disappear by examining if two or more circles intersect. For example, Fig. 1(b) presents a scenario where only two circles intersect. While the circles centered at each data point grow and more connected components are generated, holes and voids may be also created (see Fig. 1(c)). Eventually, they get filled due to increasing the radii, and the process ends when all circles intersect. The algorithmic procedure is summarized in a PD. To facilitate the visualization and preserve the geometric information, we apply the linear transformation $(b, p) = T(b, d) = (b, d - b)$ to each point in the PD. We refer to the resulting coordinates (shown as black dots and red triangles in Fig. 1(d)) as birth (b) and persistence (p), respectively, in $\mathbb{W} := \{(b, p) \in \mathbb{R}^2 \mid b, p \geq 0\}$ and call this transformed PD a tilted representation (Fig. 1 (d)).

2.2 Pairwise Interacting Point Process

In this section we describe in detail the components critical to construct the PIPP model to define the spatial distribution of persistence diagrams. One of our central motivations of the construction is to capture the local and global spatial features. A PIPP falls under the umbrella of Gibbs point process where the density function is completely determined by the first and second order potential function. In the context of PDs, the first order potential function captures the density trends of points and the second order one determines interactions between all possible pairs of points.

Let $(\mathbb{W}, \mathcal{W}, \lambda)$ be a measure space where \mathbb{W} is a bounded region in \mathbb{R}^d where a point pattern is observed, \mathcal{W} is the Borel σ algebra on \mathbb{W} and λ is the Lebesgue measure. A spatial point pattern on some region $A \in \mathcal{W}$ is defined as a set points $X = \{x_i \in A\}_{i=1}^n$. The number of points in any A has a Poisson distribution with mean $\lambda(A)$.

Definition 2.2. The pairwise interaction process on $(\mathbb{W}, \mathcal{W}, \lambda)$, has spatial pattern $s : \mathbb{W} \rightarrow \mathbb{R}^+ \cup \{0\}$ and interaction function $h_\theta : \mathbb{W} \times \mathbb{W} \rightarrow \mathbb{R}^+ \cup \{0\}$. For a spatial point pattern $\mathbf{x} = \{x_1, \dots, x_n\}$ on a region \mathbb{W} , the joint probability density has the following form

$$f(\mathbf{x}|\theta) = \frac{1}{Z(\theta)} \prod_{i=1}^n s(x_i) \prod_{i<j} h_\theta(x_i, x_j), \quad (1)$$

where

$$Z(\theta) = \int_{\mathbb{W}} \prod_{i=1}^n s(x_i) \prod_{i<j} h_\theta(x_i, x_j) d\lambda(x_1, x_2, \dots, x_n),$$

is the intractable normalizing constant.

Eqn. (1) can be written as

$$f(\mathbf{x}|\theta) = \frac{1}{Z(\theta)} \exp(U_\theta(\mathbf{x})), \quad (2)$$

where $f(\mathbf{x}|\theta)$ takes the form of the probability density of a finite Gibbs point process with potential function

$$U_\theta(\mathbf{x}) = \sum_{i=1}^n \ln(s(x_i)) + \sum_{i=1}^{n-1} \sum_{j=1}^n \ln(h_\theta(x_i, x_j)). \quad (3)$$

To model the spatial pattern s , we characterize PDs as an inhomogeneous Poisson point process with intensity $\lambda(x_i) = s(x_i)$. Here we employ a partition model based on Dirichlet tessellation to characterize the intensity. The advantage of using a partition model is that it provides a semi-automatic method of capturing the spatial structure. In a nutshell, the model partitions the space \mathbb{W} into disjoint regions and assigns a weight for each of the regions to approximate the spatial structure.

To define the local interaction between points of PDs we adopt the so called piecewise constant pairwise interaction (PCPI). This is also known as the multi-scale generalization of the Strauss process, which is the most frequently used interaction model in the literature. Nearby or distant points

in a PD represent similar or contrasting topological features, respectively. The PCPI function relies on some distance cut-offs that are considered to be appropriate for the interaction between points in a persistence diagram. PCPI is capable of extracting the level of similarity in the corresponding topological features.

Definition 2.3. The PCPI function has the form $h_\theta(x_i, x_j) = \exp(-\theta^T H(x_i, x_j))$, $x_i, x_j \in \mathbb{W}$, where $H(x_i, x_j) = (I_1(\|x_i - x_j\|), I_2(\|x_i - x_j\|), \dots, I_k(\|x_i - x_j\|))$, $I_l(\|x_i - x_j\|) := \mathbb{1}_{\{r_{l-1} < \|x_i - x_j\| < r_l\}}$, $\theta = \{\theta_l \in \mathbb{R}^+ \cup \{0\}\}_{l=0}^k$, and $0 = r_0 < r_1 < \dots < r_k$ are the parameters of the step function. Hence

$$h_\theta(x_i, x_j) = \exp\left(-\sum_{l=0}^k \theta_l \sum_{i < j} \mathbb{1}_{\{r_{l-1} < \|x_i - x_j\| < r_l\}}\right). \quad (4)$$

With the aforementioned definition of spatial tendency s , and the interaction term h_θ , we obtain the parametric model for defining the spatial structure of PDs. The cost of the associated maximum likelihood is computationally prohibitive as the normalizing constant $Z(\theta)$ is an intractable function. A standard alternative to the likelihood is the pseudolikelihood of a point process which considers the PIPP representation of PDs. The pseudolikelihood definition is based on the conditional intensity $L(u, \mathbf{x})$, which is the probability that a point process X has a point u given that X consists of the points \mathbf{x} .

Definition 2.4. The conditional intensity for a point process defined on \mathbb{W} (recall \mathbb{W} from Section 2.1) with the density f has the form,

$$L(u, \mathbf{x}) = \frac{f(\mathbf{x} \cup u)}{f(\mathbf{x})} \text{ if } u \notin \mathbf{x}$$

or,

$$L(x_i, \mathbf{x}) = \frac{f(\mathbf{x})}{f(\mathbf{x} \setminus x_i)} \text{ if } x_i \in \mathbf{x}$$

Hence for the model in Eqn. (1) we have

$$L(u, \mathbf{x}|\theta) = \exp(\theta^T (S(u) - \sum_{i=1, x_i \neq u}^n H(u, x_i))), \quad (5)$$

where $\theta = (1, \theta_1, \dots, \theta_k)$ is the parameter space and $S(u) = \ln s(u)$. Hereafter we write $\theta = (1, \theta_1, \dots, \theta_k)$ and $\theta = (\theta_1, \dots, \theta_k)$ interchangeably by abusing notation.

Definition 2.5. The pseudolikelihood of a point process with conditional intensity $L(u, \mathbf{x}|\theta)$ is defined by

$$PL(\mathbf{x}|\theta, A) = \prod_{x_i \in A} L(x_i, \mathbf{x}|\theta) \exp\left(-\int_A L(u, \mathbf{x}|\theta) du\right). \quad (6)$$

Hence the log-pseudolikelihood takes the form

$$\log PL(\mathbf{x}|\theta, A) = \sum_{i=1}^n \log L(x_i, \mathbf{x}|\theta) - \int_A L(u, \mathbf{x}|\theta) du. \quad (7)$$

The final definition we need is the Dirichlet tile to propose the quadrature scheme adapting the Berman-Turner device in [26] for approximating the parameters in Eqn. (6).

Definition 2.6. For a finite set of distinct points u_1, \dots, u_m in a metric space X , the Dirichlet tile is defined for any point $x \in X$ as $T_i = \{x : \|x - u_i\| < \|x - u_j\| \ \forall i \neq j\}$.

Hence, the Dirichlet tiles obey the property that any point in the interior of the tile T_i is closer to the point u_i than to any other point u_j whenever $i \neq j$ [27].

3 Methodology

3.1 Modeling PDs as Pairwise Interaction Model

In this section, we establish the notion of a pairwise interaction model for persistence diagrams. For this, we need to define the spatial pattern term s and the interaction function h_θ of Eqn. (1).

Spatial pattern term s . We split the wedge \mathbb{W} into m disjoint regions by following Dirichlet tiling as discussed in Def. 2.6. The Dirichlet tiling of \mathbb{W} is given by m points, say $\{p_1, \dots, p_m\} \in \mathbb{W}$, where the i -th tile, corresponding to the point p_i , contains all of the points in \mathbb{W} that are nearest in Euclidean distance to p_i than any other $p_j, j \neq i$. We assign weights on each of these points by means of the area of the respective Dirichlet tiles. We denote these weights as $\{A_1, \dots, A_m\}$ where each A_i is constant over the i -th tile. Consequently, the spatial intensity is obtained by using the area of the tiles. For example, $A(x_i)$ denotes the density at point x_i and if the point x_i is closest to the generating point p_l then the spatial intensity is $s(x_i) = A(x_i) = A_l$. For ease of notation, $(P, \mathcal{A}) := (p_1, \dots, p_m, A_1, \dots, A_m)$. In practice, the Dirichlet partition model estimates densities as the areas of Dirichlet tiles that are larger when generating points p_i have no nearby points. Consequently, in the context of PDs, the partition model estimates higher densities for higher persistence points, which carry topologically significant information of the data. We present an example of density estimation based on Dirichlet partition modeling in Section 3.1.1.

PCPI function and h_θ . The interaction between points in a PD is modeled by using the PCPI function of Def. 2.3. The interaction parameters are (k, r_0, \dots, r_k) , where k is the number of distance thresholds, and (r_0, \dots, r_k) are the distance thresholds that are considered to capture the pairwise interaction between two points x_i and x_j in a PD. Hence the pairwise interaction function $h_\theta(x_i, x_j)$ is given by Eqn. (4) of Def. 2.3.

The construction of the PCPI function proceeds by investigating pairwise distances between points and by thresholding these distances so that appropriate interactions are captured. As nearby and distant points in a PD indicate similar and contrasting topological features respectively, an appropriate interaction function should identify stronger interactions between nearby points and weaker interactions between distant points. The PCPI models interaction of points in PD at multiple scales. Precisely, the interaction between two points that are r units away in a PD is obtained by incorporating all of the component interactions that apply to the distance r . The component interactions are the instances where interaction radius, the threshold distance to consider an interaction not negligible, is more than r . An illustration of constructing the PCPI function for a PD is given in Section 3.1.1.

Pairwise interacting Gibbs model with $U_\theta(\mathbf{x})$. PDs are modeled as pairwise interacting Gibbs point processes with potential $U_\theta(\mathbf{x})$ given by Eqn. (3) using the spatial pattern s and PCPI function h_θ with the parameter space $\theta = \{\theta_1, \dots, \theta_k\}$.

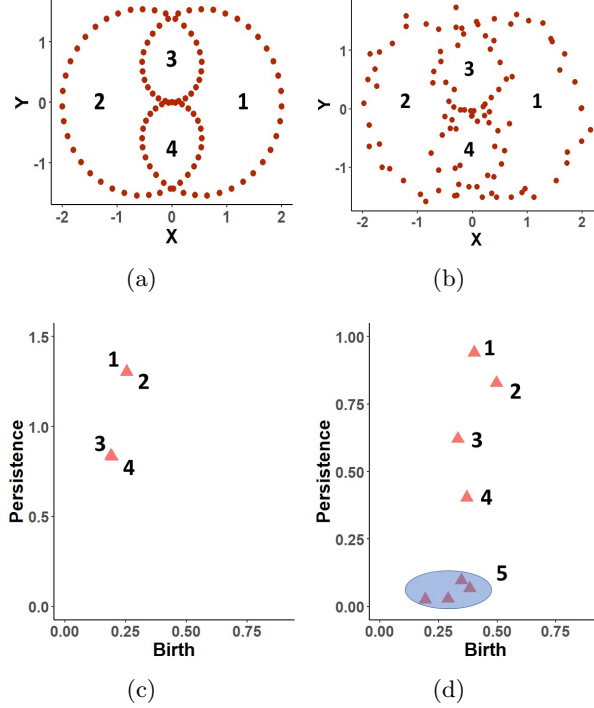


FIG. 2: (a) and (b) are random samples from a polar curve, and (c) and (d) are their corresponding persistence diagrams for 1-dimensional features. (b) is noisier than (a), consequently, their persistence diagrams show different patterns of interaction between points.

3.1.1 Example

We consider PDs generated from point clouds sampled uniformly from the polar curve (Fig. 2 (a)) and a noisy version of it (Fig 2(b)). Celtic knots, e.g. a polar curve, have been observed at electron micrographs of closed DNA and have found that these can topologically be knotted circles. We focus on estimating 1-dimensional holes, which describe the prominent topological feature of them. As the noiseless polar curve consists of two large loops and two small loops of similar sizes, the corresponding PD has four points as two pairs with overlapping points, shown in Fig. 2 (c). On the other hand, the PD generated from the noisy version of the polar curve spawns several spurious features (Fig. 2 (d)). An important phenomenon we encounter is that the two overlapping pairs in Fig. 2 (c) show a repulsive tendency in Fig. 2 (d). Furthermore, in Fig. 2 (d), the pair with the two largest persistence coordinates represents the most significant loop of the point cloud, and the pair with the second two captures the second most significant loop. Sequentially, the lowest persistence points are generated by noise, so they do not identify any significant information about

the data.

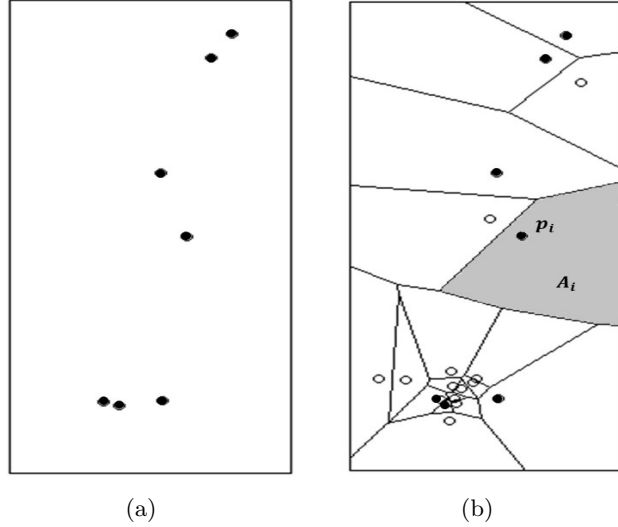


FIG. 3: (a) An example of points in a PD on the wedge \mathbb{W} . (b) Dirichlet tessellation of \mathbb{W} based on some dummy points (blank dots) and the points from PD in (a) (filled dots). The weight A_i is the area (shown as grey region) of the tile containing the point p_i .

Another noticeable phenomenon is the variation of topological features with the change in the pairwise distances. To understand this and to keep a track of particular points in the persistence diagram, we assign numbers to those points (as shown in Fig. 2 (c) and (d)). We denote the pairwise distances between points as $d_{ij} = \|i - j\|$ for $i, j = 1, \dots, 4$ and $i \neq j$. From the reference point 1, the distances are in ascending order as $d_{12} < d_{13} < d_{14} < d_{15}$ (Fig. 2 (d)). Observe that when the distance is the lowest (d_{12}), the two corresponding points 1 and 2 share the same topological features (Fig. 2 (b)). The two points 1 and 3 with the second lowest pairwise distance d_{13} share very similar features - both are loops of different sizes. Interaction between the points 1 and 4 resembles with that of 1 and 3. We cluster the noise features and present them inside of the blue oval in Fig. 2 (d). Observe that with the maximum pairwise distance d_{15} the two corresponding points 1 and any one from the blue oval are generators of significantly different features. Typically the pairwise distance between a topologically significant point with a noise point is higher than that of two topologically significant points and the interaction between a noise and a significant point is weaker. Consequently, for our analysis we considering noise points collectively which allows efficient computations.

The exposition leads us to the conjecture that the interactions between points in a PD rely on some distance thresholds that are considered to be appropriate. We construct this interaction by means of a PCPI function where the subdomain of the function is obtained from some pertinent distance thresholds. We justify the observation by computing the level of significance of interaction parameters in Section 4.

In Fig. 3, we illustrate spatial density s estimation based on the Dirichlet partition model as

discussed in Section 3.1. The data points in Fig. 3(a) are from the PD in Fig. 2(d). In practice, the Dirichlet partition model augments a list of dummy points with the data points. The dummy points can be uniformly disturbed over the specific window of consideration or can be generated from distribution. For this illustration, we simply added some points around the data points. The combined list of points is then considered to be the generating points p_i . The generating points are shown in Fig. 3(b), where filled dots represent data points and the blank dots represent dummy points. The tile T_i for each of the generating point p_i has the property that any point inside of T_i is closer to p_i than any other generating points. By computing the areas of these tiles we approximate the spatial density s .

3.2 Coefficient Parameter Estimation

In this section, we solve the parameter estimation problem to get the specific Gibbs model for the probability density function defined in Eqn. (2). An obvious choice for this is the maximum likelihood estimation. However, it is generally challenging to employ maximum likelihood approaches for point processes even for simple inhomogeneous Poisson point processes. Hence to estimate the parameters θ in the PIPP model defined in Section 3.1, we consider the pseudolikelihood in Eqn. (6). The computational device we employ to approximate the parameters that maximize the pseudolikelihood is based on [25]. Precisely, the integral in Eqn. (6) is approximated by using the Dirichlet tiling quadrature scheme. This quadrature scheme is very intuitive for PDs as the weights are associated with the area of the Dirichlet tiles. Consequently, higher weights will be assigned to the points that do not have nearby points, which are more significant to capture the underlying data structure.

We commence the process of estimating parameters in θ with an approximation of the integral in (6) by a finite sum using Dirichlet tiling based quadrature rule as

$$\begin{aligned} \int_A L(u, \mathbf{x}|\theta) du &= \int_A \exp(\theta^T(S(u) - \sum_{i=1, x_i \neq u}^n H(u, x_i))) du \\ &= \sum_{j=1}^m \exp(\theta^T(S(u_j) - \sum_{i=1, x_i \neq u_j}^n H(u_j, x_i))) w_j \end{aligned} \quad (8)$$

where $u_j, j = 1, \dots, m$, are quadrature points in $\mathbb{W} := \{(b, p) \in \mathbb{R}^2 \mid b, p \geq 0\}$, and w_j are quadrature weights. The quadrature weights are estimated as the areas of the Dirichlet tiles corresponding to the quadrature points as discussed in Section 3.1. In practice, we add dummy points in \mathbb{W} to the data points to generate u_j . There are two frequently used techniques to generate dummy points - (i) fixed $n \times n$ grid of dummy points and (ii) uniformly distributed random points on a $n \times n$ grid, i.e., each point lies in one of these grid of cells. In order to produce a more accurate result, it is always desirable to have dummy points covering the window \mathbb{W} sufficiently, however, this can increase the computational cost. Hence a trade off between computational cost and accuracy is crucial for this process.

By substituting Eqn. (8) in Eqn. (7) we get

$$\log PL(\mathbf{x}|\theta) = \sum_{i=1}^n \log L_\theta(x_i; \mathbf{x}) - \sum_{j=1}^m \exp(\theta^T(S(u_j) - \sum_{i=1, x_i \neq u_j}^n H(u_j, x_i))) w_j \quad (9)$$

According to the definition of u_j , we know that $m \geq n$. We introduce an indicator variable y_j defined as

$$y_j = y_{\mathbf{x}}(u_j) = \begin{cases} \frac{1}{w_j} & \text{if } u_j \in \mathbf{x} \\ 0 & \text{otherwise} \end{cases} \quad (10)$$

and $L_j = \exp(\theta^T(S(u_j) - \sum_{i=1, x_i \neq u_j}^n H(u_j, x_i)))$. If the list of points $\{u_j, j = 1, \dots, m\}$ includes all data points $\{x_i, i = 1, \dots, n\}$ we rewrite the Eqn. (9) as

$$\log PL(\mathbf{x}|\theta) \approx \sum_{j=1}^m (y_j \log(L_j) - L_j) w_j \quad (11)$$

The right hand side of (11) is formally equivalent to the log-likelihood of independent Poisson variable $Y_j : j = 1, \dots, m$ with respective means L_j and weights w_j . The log-pseudolikelihood in Eq. (11) induces a log-linear Poisson regression model as an approximation of the true log-likelihood.

3.3 Sampling PDs

The key contribution of this work is to define a RJ-MCMC sampling method for generating random samples of persistence diagrams modeled as pairwise interaction point processes. We propose a novel RJ-MCMC algorithm that is flexible enough to incorporate trans-dimensional addition and removal of points and same dimensional relocation of points in a PD. The goal is to generate PD with topological properties present in a given dataset. To this end, RJ-MCMC explores the PD space via three moves; (i) the points in a PD may move from one location to another without changing the total number of points, (ii) adding a point in the PD while moving from one iteration to the next, and (iii) removing a point in the PD while moving from one iteration to the next.

Our model allows flexibility in the total number of points in the sampled PDs. Also, as the likelihood estimation relies on a quadrature scheme as discussed in Section 3.2, our method can estimate statistical quantities for a PD where we only have a few numbers of points. For ease of notation, we rewrite (2) as

$$f(\mathbf{x}|\hat{\theta}) = \frac{1}{Z(\hat{\theta})} \prod_{i=1}^n s(x_i) \exp\left(\sum_{i=1}^{n-1} \sum_{j=1}^n \ln(h_{\hat{\theta}}(x_i, x_j))\right) \quad (12)$$

$$= \frac{1}{Z(\hat{\theta})} g(\mathbf{x}|\hat{\theta}) \prod_{i=1}^n s(x_i) \quad (13)$$

where $\hat{\theta} = \{\hat{\theta}_1, \dots, \hat{\theta}_k\}$ comprises of the estimated parameters of the scheme in Section 3.2.

The sampler chooses uniformly at random between three moves, namely addition, removal or relocation of points. An example of similar possibilities of transitions is illustrated in [28]. In

particular, [28] considers a state space of step functions, and allows four possible transitions; (i) changing the height of a randomly chosen step, (ii) changing the location of a chosen step, (iii) adding a new step, and (iv) removing a chosen step. Our sampling process consists of two types of MCMC updates; a Metropolis-within-Gibbs update relocates points in a PD via random-walk Metropolis steps, and an RJ-MCMC update adds points to the PD or removes points from it.

The probabilities of adding a new point, of removing a selected point, and of changing the location of a selected point are p_a , p_r , and p_m , respectively. It is assumed that $p_a + p_r + p_m = 1$. Sampling starts with an initial PD $D^{(0)} = (d_1^{(0)}, \dots, d_{|D^{(0)}|}^{(0)})$, and we choose uniformly at random among the three moves. The acceptance probabilities for these three types of moves are given in the proposition below, whose proof is available in Appendix A.

Proposition 3.1. *Consider a random PD on the wedge \mathbb{W} modeled by a PIPP with density $f(x|\hat{\theta})$ given by Eqn. (13). Density $f(x|\hat{\theta})$ is parameterized by a spatial density s and a PCPI function $h_{\hat{\theta}}$, conditional on a parameter estimate $\hat{\theta} = \{\hat{\theta}_1, \dots, \hat{\theta}_k\}$. The spatial pattern s of points in the PD is a Poisson point process with intensity λ , while the PCIP function $h_{\hat{\theta}}$ is given by Eqn. (4). Let $D^{(l)} = (d_1^{(l)}, \dots, d_{|D^{(l)}|}^{(l)})$ be the PD at the l -th MCMC iteration. The acceptance probabilities for generating random PDs from $f(x|\hat{\theta})$ by relocating, adding or removing points follow:*

- (a) *Let $D^* = (d_1^{(l)}, \dots, d_{i-1}^{(l)}, d_i^*, d_{i+1}^{(l)}, \dots, d_{|D^{(l)}|}^{(l)})$ be the candidate PD for the relocation move, where d_i^* is chosen according to a proposal density q . The acceptance probability for D^* is*

$$a(D^{(l)}, D^*) = \min \left\{ 1, \frac{s(d_i^*)g(D^*|\hat{\theta})q(d_i^{(l)})}{s(d_i^{(l)})g(D^{(l)}|\hat{\theta})q(d_i^*)} \right\}. \quad (14)$$

- (b) *For the addition of a point d^* , chosen uniformly in \mathbb{W} , to $D^{(l)}$, we consider a candidate PD $D^* = (D^{(l)}, d^*)$. The acceptance probability for D^* is*

$$a(D^{(l)}, D^*) = \min \left\{ 1, \frac{\exp \left(\sum_{i=1}^{|D^{(l)}|} \ln(h_{\hat{\theta}}(d_i^{(l)}, d^*)) \right) s(d_i^*)\lambda(\mathbb{W})}{|D^{(l)}| + 1} \right\}. \quad (15)$$

- (c) *For the removal of a point $d_i^{(l)}$ from $D^{(l)}$, we choose uniformly at random $d_i^{(l)}$ and obtain the candidate PD as $D^* = D^{(l)} \setminus d_i^{(l)}$. The acceptance probability for D^* is*

$$a(D^{(l)}, D^*) = \min \left\{ 1, \frac{|D^{(l)}|}{\exp \left(\sum_{j \neq i} \ln(h_{\hat{\theta}}(d_j^{(l)}, d_i^{(l)})) \right) s(d_i^{(l)})\lambda(\mathbb{W})} \right\}. \quad (16)$$

The pseudocode of the MCMC sampler for generating PDs is outlined in Algorithm 1. One key research question for generating random PDs represented by a spatial point process would be what are the appropriate transitions. In developing our sampler for PDs, we have considered three plausible scenarios; (i) samples obtained by using relocation, addition and removal of points, (ii) samples obtained by using addition and removal of points only, and (iii) samples obtained by using relocation of points only. We present the results of the chosen scenario (i) in Section 4 and the results for the other two scenarios in Appendix B.

Algorithm 1 RJ-MCMC sampling of PDs

```
1: Input: Initial PD  $D^{(0)} = (d_1^{(0)}, \dots, d_{|D^{(0)}|}^{(0)})$  and probabilities  $(p_a, p_r, p_m)$ 
2:
3: for  $l \in \{1, \dots, N\}$  do
4:   Sample  $\gamma \in \{1, 2, 3\}$  from  $\gamma \sim \text{Categorical}(p_a, p_r, p_m)$ 
5:
6:   if  $\gamma = 1$  then
7:     Sample  $d^*$  uniformly at random in  $\mathbb{W}$ 
8:      $D^* = (D^{(l)}, d^*)$ 
9:     Compute  $a(D^{(l)}, D^*)$  from Eqn. (15)
10:    Sample  $u$  from uniform  $\mathcal{U}(0, 1)$ 
11:    if  $u < a(D^{(l)}, D^*)$  then
12:       $D^{(l+1)} = D^*$ 
13:       $|D^{(l+1)}| = |D^{(l)}| + 1$ 
14:    end if
15:  else if  $\gamma = 2$  then
16:    Sample a point  $d_i^*$  from  $D^{(l)}$ 
17:     $D^* = D^{(l)} \setminus d_i^{(l)}$ 
18:    Compute  $a(D^{(l)}, D^*)$  from Eqn. (16)
19:    Sample  $u$  from uniform  $\mathcal{U}(0, 1)$ 
20:    if  $u < a(D^{(l)}, D^*)$  then
21:       $D^{(l+1)} = D^*$ 
22:       $|D^{(l+1)}| = |D^{(l)}| - 1$ 
23:    end if
24:  else
25:    for  $i = 1$  to  $|D^{(l)}|$  do
26:      Sample  $d_i^*$  according to a proposal density  $q$ 
27:       $D^* = (d_1^{(l)}, \dots, d_{i-1}^{(l)}, d_i^*, d_{i+1}^{(l)}, \dots, d_{|D^{(l)}|}^{(l)})$ 
28:      Compute  $a(D^{(l)}, D^*)$  from Eqn. (14)
29:      Sample  $u$  from uniform  $\mathcal{U}(0, 1)$ 
30:      if  $u < a(D^{(l)}, D^*)$  then
31:         $D^{(l+1)} = D^*$ 
32:      end if
33:    end for
34:  end if
35: end for
```

4 Examples

In this section, we present some examples to (i) generate samples of PDs by using the RPDG technique of Section 3, (ii) illustrate the estimation of the parameters using the algorithm discussed in Section 3.2, (iii) demonstrate the utility of PIPP modeling for PDs with PCPI interaction function, and (iv) compare the results obtained by using the RPDG technique with two existing methods [21–23]. We consider point clouds sampled from the polar curve of Example 3.1.1 and confine our analysis to 1-dimensional holes of the corresponding PDs, which describe the prominent topological signatures of the polar curve.

4.1 RPDG Illustration

First, we discuss how we implement the RPDG technique to generate 1000 samples of the PD (Fig. 2 (d)) of the noisy version of the polar curve Fig. (2 (b)) generated by Vietoris Rips filtration. We used the Dirichlet partition model to define the spatial pattern term s . The Dirichlet partition model can be carried out on the whole plane, which is unattainable. In practice, the partitioning is computed within a restricted window that contains all data points under consideration. We selected the restricted window to be $W = [0, 1] \times [0, 1]$ as all of the points in the original PD (Fig. 2 (d)) fall within this window.

Next we sampled 20 dummy points from the Gaussian mixture $\sum_{i=1}^3 c_i \mathcal{N}(\mu_i, \sigma_i)$ with $(c_1, c_2, c_3) = (1, 1, 6)$, $(\mu_1, \mu_2, \mu_3) = ((0.6, 0.85), (0.4, 0.6), (0.3, 0.01))$, and $(\sigma_1, \sigma_2, \sigma_3) = (0.001, 0.001, 0.001)$. The choice of the parameters in the Gaussian mixture was motivated by the three clusters in the original PD. The means μ_i were chosen to be the center of the clusters and the weights c_i with a relatively higher value for the third component was due to the fact that low persistence holes were rare events arising from noise. We augmented the 8 data points of the original PD by 20 dummy points and created a set of $m = 28$ points to perform Dirichlet tiling. A sample of dummy points is shown in Fig. 4. Finally we split the window W into m disjoint regions or tiles corresponding to points $P = \{p_i\}_{i=1}^m$, where the i -th tile corresponds to the point p_i and contains all of the points inside of W that are closest to p_i in Euclidean distance than any other points in P .

In order to define the PCPI function h_θ , we relied on empirical/experimental knowledge for the choice of parameters $\{k, r_0, \dots, r_k\}$. Observe that in the original PD (Fig. 2 (d)) the pairwise distances range from 0 to $1 + \epsilon$ for some small $\epsilon > 0$. Consequently we divide this range into $\{0, 0.1, 0.2, \dots, 1\}$. We selected $\{r_0, \dots, r_k\} = \{0, 0.1, 0.2, 0.3\}$ empirically. In particular, r_i were selected so that corresponding parameters θ_i are significant for the PIPP modeling of the PD. We provide more details in Section 4.1.1. Furthermore, the choice of thresholds r_i agrees with the fact that there are three clusters in the original PD, implying $k = 3$.

4.1.1 Estimated Coefficient Parameters:

Here we estimated the coefficient parameters $\hat{\theta} = \{\hat{\theta}_1, \dots, \hat{\theta}_k\}$ by using the method discussed in Section 3.2. Precisely our goals are to: (i) check the validity of the model's interaction parameters $\{r_i\}_{i=1}^k$ by means of the significant associations between their corresponding terms with coefficient

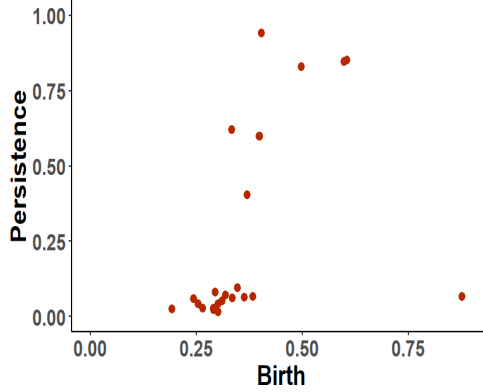


FIG. 4: Example of 20 dummy points sampled from Gaussian mixture $\sum_{i=1}^3 c_i \mathcal{N}(\mu_i, \sigma_i)$ with $(c_1, c_2, c_3) = (1, 1, 6)$, $(\mu_1, \mu_2, \mu_3) = ((0.6, 0.85), (0.4, 0.6), (0.3, 0.01))$, and $(\sigma_1, \sigma_2, \sigma_3) = (0.001, 0.001, 0.001)$.

θ_i and the response terms y_j in Eqn. (11), and (ii) assess the reliability of the parameter estimation by computing confidence intervals.

In order to check the validity of the interaction parameters $\{r_i\}_{i=1}^k$, we estimated the corresponding coefficient parameters θ_i and performed the hypothesis test where the null hypothesis is that the term in the model with coefficient parameter θ_i is not significant for the model. We employed a significance level of 0.05. With $r = \{0.1, 0.2, 0.3\}$, the estimated parameters and their corresponding p -values are listed in Table 1. Observe that all of the estimated parameters are highly significant with very low p -values. We experimented empirically with different r threshold values and obtained this choice with the maximum significant associations.

Parameter	Estimation		
	Mean	CI	p value
θ_1	0.3153	[0.2983, 0.3324]	2.00e-16
θ_2	0.3166	[0.2504, 0.3828]	4.28e-08
θ_3	0.3340	[0.0997, 0.5684]	2.00e-16

TABLE 1: The means and 95% confidence intervals (CIs) for the three estimated parameters that maximize log-pseudolikelihood in Eq. (11) obtained by fitting the loglinear Poisson regression model associated with the Berman-Turner computational device. The corresponding p -values to indicate their significance levels.

Next, we tested the robustness of the estimated parameters $\hat{\theta}$. For this, we sampled 100 sets of point clouds from the polar curve function, added Gaussian noise with the 2×2 covariance matrix $0.01I_2$ and computed the associated PD for each set of point clouds. We then estimated the coefficient parameters by following the technique in Section 3.2 for each of the 100 PDs. For this analysis, we preselected the interaction thresholds as $\{r_1, r_2, r_3\} = \{0.1, 0.2, 0.3\}$. The means

and 95% confidence intervals were also estimated as presented in Table 1. The robustness of these estimations is evident from the confidence intervals.

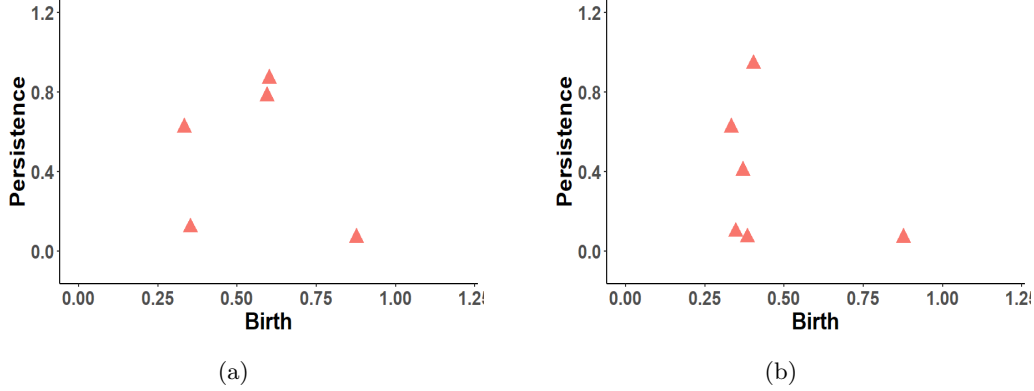


FIG. 5: Randomly generated PDs after (a) 100 and (b) 500 simulations using the RPDG.

Finally, we use the coefficient estimator $\hat{\theta}$ to generate 1,000 samples of PDs using Algorithm 1 with move probabilities $p_a = 0.35$, $p_r = 0.35$, and $p_m = 0.3$. The proposal distribution q is considered to be the Gaussian mixture density $\sum_{i=1}^3 c_i \mathcal{N}(\mu_i, \sigma_i)$ with $(c_1, c_2, c_3) = (1, 1, 6)$, $(\mu_1, \mu_2, \mu_3) = ((0.6, 0.85), (0.4, 0.6), (0.3, 0.01))$, and $(\sigma_1, \sigma_2, \sigma_3) = (0.001, 0.001, 0.001)$. Two instances after 100 and 500 simulations are presented in Fig. 5. One of the central motivations to estimate samples of PDs is to differentiate topological noise from topological signals. In order to agree with the preexisting statistical inferences performed with the samples of PDs, we followed the method showed in [23] to estimate the confidence intervals for PDs. Naively, the points in the persistence diagram that have longer persistence are considered topologically significant. Consequently, the quantities of interest for this analysis are the highest persistence points and we define them as O_i , the i -th largest persistence points.

Statistic	Original value	CI	P_i value
O_1	0.9409	[0, 0.8597]	$2.20e - 16$
O_2	0.8284	[0, 0.7168]	$2.20e - 16$
O_3	0.6207	[0, 0.5454]	$5.80e - 13$
O_4	0.4035	[0, 0.3580]	$4.68e - 05$
O_5	0.0962	[0, 0.1819]	$1.00e - 00$

TABLE 2: The confidence intervals for the first five order statistics of 1,000 generated samples of PDs using RPDG. The underlying point cloud consists of four loops and the first four order statistics represent them. Note that all of the O_i^{org} are outside of the one-sided 5% confidence intervals, hence, they are all topologically significant.

The empirical distribution \mathbb{P}_i^* of O_i was obtained over 1,000 RJ-MCMC iterations. For a

random variable O , let $a_i = \inf\{a \geq 0 : \mathbb{P}_i^*(O \geq O_i^{org} + a) \leq \alpha\}$, and the i -th largest persistence point in the original PD be O_i^{org} . Therefore the one sided $100(1 - \alpha)\%$ confidence interval of the estimated value of O_i , namely \hat{O}_i has the form $[0, \hat{O}_i + a_i]$. The outcome of estimating the confidence interval is that whenever a point in the PD falls outside of the confidence interval, it is categorized as topologically significant. We tested the null hypothesis that the order statistics O_i is not topologically significant [23]. In particular, we estimated the probability $P_i = \mathbb{P}_i^*(O > O_i^{org})$, where a very small value of P_i indicates that the point O_i is highly significant. The process was conducted sequentially as in [23], that is we proceeded with the analysis of the order statistics O_{i+1} only if O_i is topologically significant.

The 5% one sided confidence intervals for the first five order statistics are shown in Table 3. All of the first four order statistics are highly significant. This agrees with the underlying structure of the data set accurately as it comprises two larger and two smaller loops, i.e, four topologically significant 1-dimensional features. The fifth order statistics arises from a noise and the confidence interval allows us to identify that correctly.

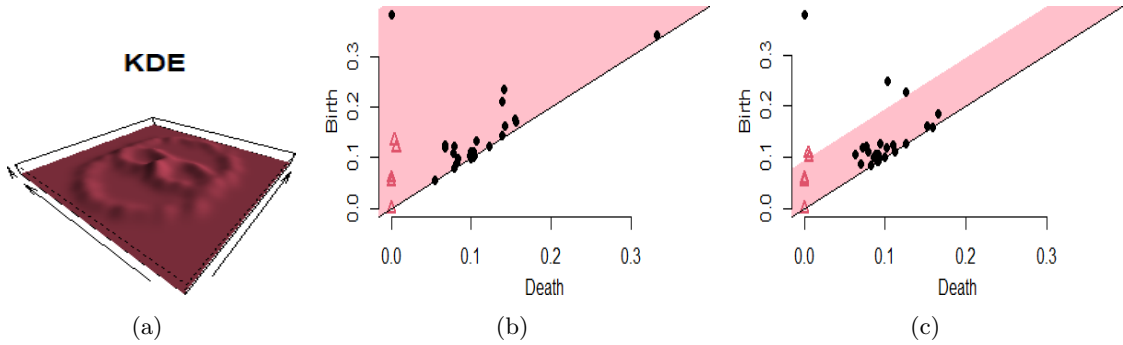


FIG. 6: (a) shows the kernel density estimator with bandwidth $h = 0.15$ of the polar curve in Fig. 2 (b). (b) shows the confidence band for corresponding persistence diagrams generated by level set filtration using the method in [21]. (c) shows the confidence band of the same persistence diagrams using the method in [22]. We use 100 bootstrap iterations here.

4.2 Bootstrap based sampling method

Bootstrap based subsampling methods to compute statistics, such as confidence sets of the subsamples of PDs, are proposed in [21, 22]. These works are significant additions to the existing literature for statistical inferences of PDs. The visualization of confidence sets in both [21] and [22] are simple and intuitive. By means of bottleneck norm, [21] computes $100(1 - \alpha)\%$ confidence band around the diagonal and establishes results to prove that points of a PD that fall in its $100(1 - \alpha)\%$ confidence band should not be considered as topologically significant. For the comparison with this subsampling based confidence set method, we return to the polar curve of Section 4.1.

The kernel density estimator (KDE) of the of the polar curve in Fig. 2 (b) is shown in Fig. 6 (a). The PD is generated by using sublevel set filtration of the KDE. We computed the confi-

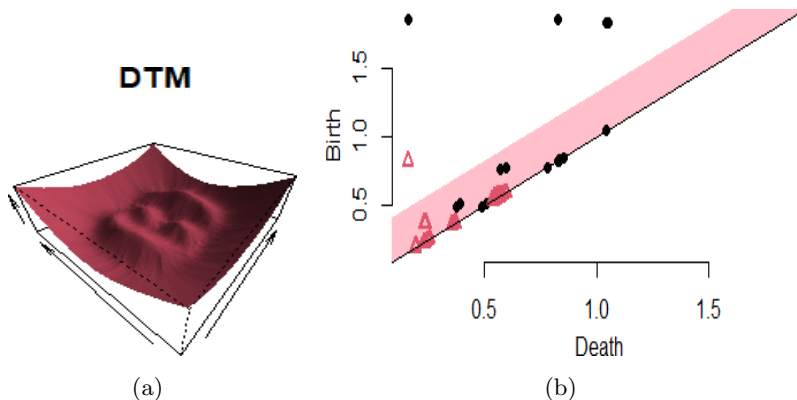


FIG. 7: (a) shows the DTM smooth function of the polar curve in Fig. 2 (b). The smoothing parameter for DTM is $m_0 = 0.08$. (b) shows the confidence band for corresponding persistence diagrams generated by level set filtration using the method in [22]. We use 100 bootstrap iterations here.

dence band at the level of $\alpha = 0.05$ and bandwidth $h = 0.15$ of the corresponding PD and the result is shown in Fig. 6 (b) using the bootstrap based method in [21]. However, none of the significant 1-dimensional homological features has been identified by using the method. The study in [22] implements the bottleneck based bootstrap method directly on the persistence diagrams constructed through the super-level sets of the KDE. As opposed to the work of [21], the algorithm proposed by [22] finds different confidence bands for different homological features. Applying this technique to the persistence diagrams of the polar curve, we computed the confidence bands for 1-dimensional homological features only. We observe in Fig. 2 (c) that the technique successfully captures the highest persistent feature as significant and marginally identifies the second highest feature. However it fails to capture two other topologically significant 1-dimensional homological features, i.e., loops. We also implemented the distance-to-measure (DTM) smooth function and the bottleneck based bootstrap method [22] to estimate the confidence bands for 1-dimensional homological features. The DTM function of the polar curve (Fig. 2 (c)) is shown in Fig. 7 (a) and the corresponding confidence band in Fig. 7 (b). The corresponding confidence band is able to identify the highest persistence point accurately. However, it fails to identify the other loops of the polar curve.

4.3 Gibbs model based MCMC sampling

A Metropolis-within-Gibbs sampling scheme for persistent homology is proposed in [23]. This work is also an important addition to the simulation of persistence diagrams literature as well as for solving statistical inference problems with PDs. The authors generate a sequence of PDs keeping the number of points fixed, see Algorithm 2 for sampling scheme.

For the sake of comparison, we consider the noisy version of the polar curve in Fig. 2 (b) and the corresponding PD with 1-dimensional features only as shown in Fig. 2 (d). In particular,

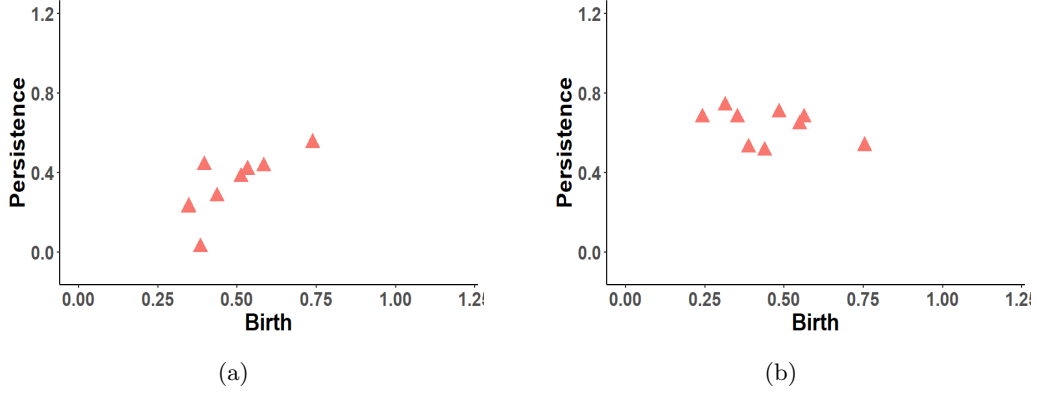


FIG. 8: Randomly generated PDs after (a) 100 and (b) 500 simulations using the MCMC sampling method of [23, 24].

we prefer this example to investigate the nature of 1-dimensional features, i.e., holes. The 1-dimensional features of the PD consists of two disjoint high persistent clusters (see Fig. 2(d)). Each of these clusters entails features of varying levels of significance in the dataset and exhibits strong interactions with others. For this type of curve, the connected component information will not be sufficient to capture the underlying data structure alone. By using the Metropolis-within-Gibbs sampling scheme we realize 1,000 samples of PDs and present two examples from that array of samples in Fig. 8. We then compute the confidence interval for several order statistics as in [23]. Readers are referred to Section 4.1 for details about confidence interval computation.

The results of the confidence intervals of the first five order statistics $\{O_1, \dots, O_5\}$ obtained from 1000 samples of PDs are presented in Table 3. Notice that the confidence intervals and the probability estimation for the first two order statistics O_1 and O_2 indicate the topological significance accurately. However, the third and fourth order statistics seems to be not significant. The underlying structure of the data, that is four loops, requires identifying the first four order statistics to be topologically significant and the sampling approach fails to achieve that. We present the fifth order statistics to show that the method can accurately pick this as a noise feature.

Statistic	Original value	CI	P _i value
O_1	0.940924	[0, 0.7156]	$2.20e - 16$
O_2	0.828386	[0, 0.6550]	$2.20e - 16$
O_3	0.620711	[0, 0.6232]	$0.90e - 00$
O_4	0.403530	[0, 0.42250]	$1.00e - 00$
O_5	0.096277	[0, 0.29540]	$1.00e - 00$

TABLE 3: The confidence intervals for the first five order statistics of 1,000 generated samples of PDs using the method in [24]. The underlying point cloud consists of four loops and the first four order statistics represent them. Note that only first two order statistics are outside of the one-sided 5% confidence intervals, hence, the other order statistics are not considered as topologically significant here.

5 Conclusion

A parametric approach to generating random persistence diagrams has been presented. This consists of modeling persistence diagrams using a pairwise interacting point process, as well as an efficient parameter estimation method by means of the Dirichlet quadrature scheme. Our RPDG sampling introduces the *first* reversible jump MCMC technique for topological summaries. The RJ-MCMC sampling scheme crucially includes three types of moves, namely adding a new point, removing a selected point, changing the location of a selected point. Consequently, the proposed method is flexible enough to accommodate the randomness in the location of points and number of points, thus sampling PDs with topological features present in the original PDs.

The spatial intensity of the PIPP model of PDs is quantified by a Dirichlet partition model. This provides a semi-automatic method to compute the density relying on the aspect that higher persistence points are assigned with higher intensity. Two different paths can be taken for employing the Dirichlet partition model; (i) Dirichlet tile with a fixed number of tiles and (2) Dirichlet tile with a varying number of tiles. In our analysis, we use the former one for obvious reasons; in order to pursue a Dirichlet tiling with varying number of tiles, we need to incorporate at least one additional dimension in the parameter space. In particular, we need to include an additional RJ-MCMC move, according to which the number of tiles changes with probability p_t or remains the same with probability $1 - p_t$. We will explore this direction in a future publication.

We compare the output of our algorithm with two other existing approaches present in the literature to generate random PDs, based on subsampling or on Metropolis-within-Gibbs sampling. However, statistics obtained from a subsample may lose important information. Also, the Metropolis-within-Gibbs sampler relies on the restrictive algorithmic choice that the number of total points in a PD remains the same throughout all iterations. Our results outperform both of these methods.

Acknowledgements

The work has been partially supported by the ARO W911NF-17-1-0313 (FN, VM), W911NF-21-1-0094 (VM); NSF DMS-1821241 (VM), DMS-2012609 (VM), and ARL Co-operative Agreement # W911NF-19-2-0328 (VM). The views and conclusions contained in this document are those of the authors and should not be interpreted as representing the official policies, either expressed or implied, of the Army Research Laboratory or the U.S. Government. The U.S. Government is authorized to reproduce and distribute reprints for Government purposes not withstanding any copyright notation herein.

Appendix

A Proof of Proposition 3.1

To prove Proposition 3.1 we use a result about simulation method for spatial point processes given below; for more details, the reader may refer to [29].

Lemma 5.1. *To simulate a spatial point process that has a density f and the number of points in the point process on a region A has a Poisson distribution with mean $\lambda(A)$. Denote the initial point pattern as \mathbf{x} with n number of points. Consider the new point ζ having the distribution $\frac{\lambda(\cdot)}{\lambda(A)}$ so that the candidate point pattern is $\mathbf{y} = \mathbf{x} \cup \zeta$. We accept the point pattern \mathbf{y} with the acceptance probability*

$$\alpha_{add} = \frac{f(y)\lambda(A)}{f(x)(n+1)}. \quad (17)$$

If $\mathbf{x} = \emptyset$ then the chain stays at \mathbf{x} . Otherwise to remove a point, we choose $\zeta \in \mathbf{x}$ randomly and set the candidate point pattern $\mathbf{y} = \mathbf{x} \setminus \zeta$. Consequently, we accept the point pattern \mathbf{y} with the acceptance probability

$$\alpha_{remove} = \frac{f(y)n}{f(x)\lambda(A)}. \quad (18)$$

of Proposition 3.1. We commence the proof by denoting the acceptance probability as $a(D^{(l)}, D^*) = \min \{1, R(D^{(l)}, D^*)\}$. The initial PD is given as $D^{(l)} = (d_1^{(l)}, \dots, d_{|D^{(l)}|}^{(l)})$ for $l = 0$. For the relocation move, we implement Metropolis-within-Gibbs update where each point d_i in a PD is relocated by choosing a random point d_i^* according to the proposal density q to obtain the candidate PD $D^* = (d_1^{(l)}, \dots, d_{i-1}^{(l)}, d_i^*, d_{i+1}^{(l)}, \dots, d_{|D^{(l)}|}^{(l)})$. We obtain the following form of $R(D^{(l)}, D^*)$:

$$R(D^{(l)}, D^*) = \frac{f(D^*|\hat{\theta})q(d_i^{(l)})}{f(D^{(l)}|\hat{\theta})q(d_i^*)} = \frac{Z(\hat{\theta})g(D^*|\hat{\theta})[\prod_{j \neq i} s(d_j^{(l)})]s(d_i^*)q(d_i^{(l)})}{Z(\hat{\theta})g(D^{(l)}|\hat{\theta})\prod_{j=1}^{|D^{(l)}|} s(d_j^{(l)})q(d_i^*)}.$$

Hence the acceptance probability for relocation move in Eqn. (14) follows from the above equation. The proof of the identities in Eqn. (15) and (16) follows from the Lemma 5.1. For the addition move, we set a candidate PD $D^* = (D^{(l)}, d^*)$ where d^* is chosen randomly on \mathbb{W} . Eqn. (17)

indicates that we select D^* as $D^{(l+1)}$ with $|D^{(l+1)}| = |D^{(l)}| + 1$ with probability $a(D^{(l)}, D^*)$ where

$$\begin{aligned}
R(D^{(l)}, D^*) &= \frac{f(D^*|\hat{\theta})\lambda(\mathbb{W})}{f(D^{(l)}|\hat{\theta})(|D^{(l)}| + 1)} \\
&= \frac{Z(\hat{\theta})g(D^*|\hat{\theta})s(d^*)[\prod_{j=1}^{|D^{(l)}|} s(d_j^{(l)})]\lambda(\mathbb{W})}{Z(\hat{\theta})g(D^{(l)}|\hat{\theta})\prod_{j=1}^{|D^{(l)}|} s(d_j^{(l)})(|D^{(l)}| + 1)} \\
&= \frac{f(D^{(l)}|\hat{\theta})s(d^*)\exp(\sum_{i=1}^{|D^{(l)}|} \ln(h_\theta(d_i^{(l)}, d^*)))\lambda(\mathbb{W})}{f(D^{(l)}|\hat{\theta})(|D^{(l)}| + 1)} \\
&= \frac{\exp(\sum_{i=1}^{|D^{(l)}|} \ln(h_\theta(d_i^{(l)}, d^*)))s(d_i^*)\lambda(\mathbb{W})}{|D^{(l)}| + 1}.
\end{aligned}$$

This completes the proof of the acceptance probability for addition move in Eqn. (15). Finally in order to remove a selected point $d_i^{(l)} \in D_i^{(l)}$, we set the candidate PD as $D^* = D^{(l)} \setminus d_i^{(l)}$. Similarly by following Eqn. (18) accept the candidate PD when $R(D^{(l)}, D^*)$ takes the following form.

$$\begin{aligned}
R(D^{(l)}, D^*) &= \frac{f(D^*|\hat{\theta})(|D^{(l)}|)}{f(D^{(l)}|\hat{\theta})\lambda(\mathbb{W})} \\
&= \frac{Z(\hat{\theta})g(D^*|\hat{\theta})\prod_{j \neq i} s(d_j^{(l)})(|D^{(l)}|)}{Z(\hat{\theta})g(D^{(l)}|\hat{\theta})\prod_{j=1}^{|D^{(l)}|} s(d_j^{(l)})\lambda(\mathbb{W})} \\
&= \frac{f((D^{(l)} \setminus d_i^{(l)})|\hat{\theta})|D^{(l)}|}{f(D^{(l)}|\hat{\theta})\lambda(\mathbb{W})} \\
&= \frac{|D^{(l)}|}{\exp(\sum_{j \neq i} \ln(h_\theta(d_j^{(l)}, d_i^{(l)})))s(d_i^{(l)})\lambda(\mathbb{W})}.
\end{aligned}$$

Hence this complete the proof of the acceptance probability for removal move in Eqn. (16)

□

B Designing the RJ-MCMC

Here we present two other plausible scenarios we considered for designing the RJ-MCMC samplers in Algorithm 1: (i) samples obtained by using relocation of points only, and (ii) samples obtained by using addition and removal of points. Our goal is to provide a heuristic justification to the choice of all three moves in the RJ-MCMC samples. For each of these scenarios we computed 1000 samples of PDs and performed statistical inference by estimation confidence intervals as in Section 4.1.

B.1 Relocation of points only

With the relocation of points only move, the model reduced to a straightforward Metropolis-within-Gibbs sampling method. For completeness, we present the pseudocode used for this analysis as

Algorithm 2 Metropolis-within-Gibbs sampling of persistence diagrams

```

1: Input: Initial PD  $D^{(0)} = (d_1^{(0)}, \dots, d_{|D^{(0)|}}^{(0)})$ 
2: for  $l \in \{1, \dots, N\}$  do
3:   for  $i = 1$  to  $|D^{(l)}|$  do
4:     Choose  $d_i^*$  according to a proposal density  $q$ 
5:      $D^* = (d_1^{(l)}, \dots, d_{i-1}^{(l)}, d_i^*, d_{i+1}^{(l)}, \dots, d_{|D^{(l)}|}^{(l)})$ 
6:     Compute  $a(D^{(l)}, D^*)$  from Eqn. (14)
7:     Sample  $u$  from uniform  $\mathcal{U}(0, 1)$ 
8:     if  $u < a(D^{(l)}, D^*)$  then
9:       Set  $D^{(l+1)} = D^*$ 
10:    end if
11:  end for
12: end for

```

Algorithm 2. Two instances of the estimated PD samples after 100 and 500 iterations are presented in Fig. 9. The confidence intervals for the estimations of first five order statistics $\{O_i\}_{i=1}^5$ are listed in Table 4.

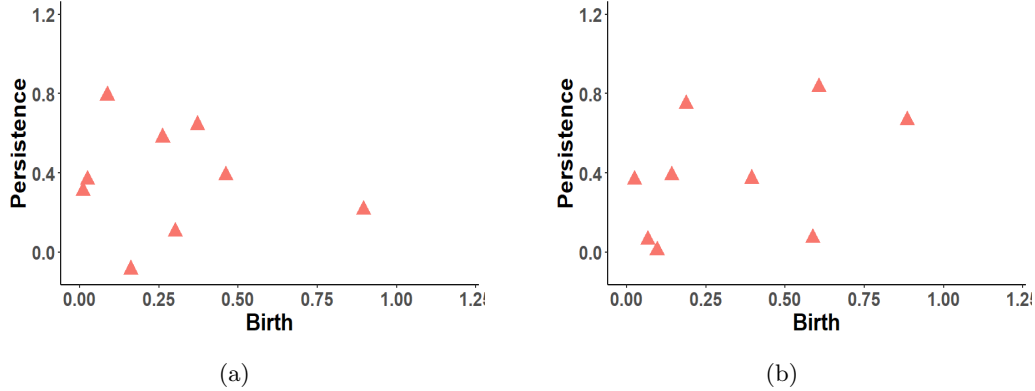


FIG. 9: Simulations of a PD arising from the polar curve in Section 4.1 using Algorithm 2 after (a) 100 and (b) 500 steps.

Observe that the confidence intervals obtained by using Algorithm 2 are able to identify the first two order statistics correctly. By the same token, they consider the third, fourth and fifth order statistics as topological noise. This demonstrates that the proposed RJ-MCMC sampler outperforms Metropolis-within-Gibbs sampling in terms of topological feature detection.

B.2 Addition and removal of points only

First we explain the alterations needed in Algorithm 1 for this exposition. Due to the requirement of two moves of adding a new point and removing a selected point only, we sample $\gamma \in \{1, 2\}$ from

Statistic	Original value	CI	P _i value
O_1	0.940924	[0, 0.8860]	$1.02e - 14$
O_2	0.828386	[0, 0.7409]	$2.17e - 15$
O_3	0.620711	[0, 0.5816]	$3.00e - 02$
O_4	0.403530	[0, 0.4028]	$0.94e - 00$
O_5	0.096277	[0, 0.2884]	$1.00e - 00$

TABLE 4: The confidence intervals of the first five order statistics of 1,000 generated samples of PDs using Algorithm 2. The first two order statistics are identified as topologically significant.

$\gamma \sim \text{Categorical}(p_a, p_r)$ in step 3. One can trivially set both of the two probabilities p_a and p_r to be 0.5. We skipped the steps from 25-33 as they are designed for the relocation move. Two instances of the estimated PD samples after 100 and 500 iterations are presented in Fig. 10. The confidence intervals for the estimations of first five order statistics $\{O_i\}_{i=1}^5$ are listed in Table 5. Observe that the confidence intervals can successfully identify the first three of the topological signatures. The confidence interval corresponding to the fourth order statistics is unable to categorize this topological feature as significant. Indeed this example demonstrates empirically that neither the relocation only based sampling in Section B.1 nor the addition and removal only based sampling in this Section (B.2) can sufficiently serve the purpose of distinguishing topological signatures from topological noise. On the other hand, the proposed RJ-MCMC PD sampling scheme of this paper, which includes trans-dimensional addition and removal of points and same-dimensional relocation of points across samples of PDs, is effective in terms of identifying significant topological features.

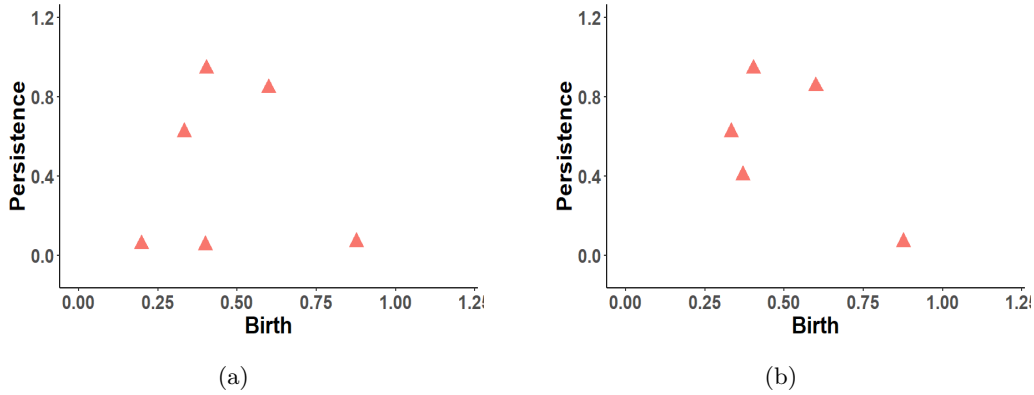


FIG. 10: Simulations of a PD arising from the polar curve using the variant of RPDG as discussed in Section B.2 after (a) 100 and (b) 500 steps.

Statistic	Original value	CI	P_i value
O_1	0.940924	$[0, 0.8789]$	$2.20e - 16$
O_2	0.828386	$[0, 0.7314]$	$2.20e - 16$
O_3	0.620711	$[0, 0.5909]$	$2.64e - 03$
O_4	0.403530	$[0, 0.3432]$	$9.95e - 01$
O_5	0.096277	$[0, 0.2406]$	$1.00e - 00$

TABLE 5: The confidence intervals for the first five order statistics of 1,000 generated samples of PDs using addition and removal moves only of RPDG. The first three prominent loops are identified as topologically significant.

References

- [1] H. Edelsbrunner and J. L. Harer. *Computational topology: an introduction*. American Mathematical Society, Providence, R.I., 2010.
- [2] V. Patrangenu, P. Bubenik, R. L. Paige, and D. Osborne. Topological data analysis for object data. *arXiv:1804.10255*, 2018.
- [3] Wei Guo, Krithika Manohar, Steven L. Brunton, and Ashis G. Banerjee. Sparse-TDA: Sparse realization of topological data analysis for multi-way classification. *IEEE Transactions on Knowledge and Data Engineering*, 30(7):1403 – 1408, 2018.
- [4] Ephy R. Love, Benjamin Filippenko, Vasileios Maroulas, and Gunnar Carlsson. Topological deep learning. *arXiv:2101.05778*, 2021.
- [5] C. A.N. Biscio and J. Møller. The accumulated persistence function, a new useful functional summary statistic for topological data analysis, with a view to brain artery trees and spatial point process applications. *Journal of Computational and Graphical Statistics*, pages 1537–2715, 2019.
- [6] F. Nasrin, C. Oballe, D. L. Boothe, and V. Maroulas. Bayesian topological learning for brain state classification. In *Proceedings of 2019 IEEE International Conference on Machine Learning and Applications (ICMLA)*, 2019.
- [7] V. Maroulas, J. L. Mike, and C. Oballe. Nonparametric estimation of probability density functions of random persistence diagrams. *Journal of Machine Learning Research*, 20(151):1–49, 2019.
- [8] Firas A. Khasawneh and Elizabeth Munch. Chatter detection in turning using persistent homology. *Mechanical Systems and Signal Processing*, 70–71:527 – 541, 2016.
- [9] A. Marchese and V. Maroulas. Signal classification with a point process distance on the space of persistence diagrams. *Advances in Data Analysis and Classification*, 12(3):657–682, 2018.

- [10] Vasileios Maroulas, Farzana Nasrin, and Christopher Oballe. A Bayesian framework for persistent homology. *SIAM Journal on Mathematics of Data Science*, 2(1):48–74, 2020.
- [11] Jacob Townsend, Cassie Putman Micucci, John H. Hymel, Vasileios Maroulas, and Konstantinos D. Vogiatzis. Representation of molecular structures with persistent homology for machine learning applications in chemistry. *Nat Commun*, 11:3230, 2020.
- [12] D. P. Humphreys, M. R. McGuirl, M. Miyagi, and A. J. Blumberg. Fast estimation of recombination rates using topological data analysis. *GENETICS*, 2019.
- [13] Y. Mileyko, S. Mukherjee, and J. Harer. Probability measures on the space of persistence diagrams. *Inverse Problems*, 27(12):124007, 2011.
- [14] Elizabeth Munch, Katharine Turner, Paul Bendich, Sayan Mukherjee, Jonathan Mattingly, and John Harer. Probabilistic fréchet means for time varying persistence diagrams. *Electron. J. Statist.*, 9(1):1173–1204, 2015.
- [15] K. Turner, Y. Mileyko, S. Mukherjee, and J. Harer. Fréchet means for distributions of persistence diagrams. *Discrete and Computational Geometry*, 52(1):44–70, 2014.
- [16] Omer Bobrowski, Sayan Mukherjee, and Jonathan E. Taylor. Topological consistency via kernel estimation. *Bernoulli*, 23(1):288–328, 2017.
- [17] F. Chazal, V. de Silva, and S. Oudot. Persistence stability for geometric complexes. *Geometriae Dedicata*, 173(1):193–214, 2014.
- [18] Andrew J. Blumberg, Itamar Gal, Michael A. Mandell, and Matthew Pancia. Persistent homology for metric measure spaces, and robust statistics for hypothesis testing and confidence intervals. *Found. Comput. Math.*, 4:1–45, 2014.
- [19] Frédéric Chazal, Brittany Terese Fasy, Fabrizio Lecci, Alessandro Rinaldo, and Larry Wasserman. Stochastic convergence of persistence landscapes and silhouettes. In *Proceedings of the thirtieth annual symposium on Computational geometry*, pages 474–483, 2014.
- [20] A. Robinson and K. Turner. Hypothesis testing for topological data analysis. *Journal of Applied and Computational Topology*, 1(2):241–261, 2017.
- [21] Brittany Terese Fasy, Fabrizio Lecci, Alessandro Rinaldo, Larry Wasserman, Sivaraman Balakrishnan, Aarti Singh, et al. Confidence sets for persistence diagrams. *The Annals of Statistics*, 42(6):2301–2339, 2014.
- [22] Frédéric Chazal, Brittany Fasy, Fabrizio Lecci, Bertrand Michel, Alessandro Rinaldo, Alessandro Rinaldo, and Larry Wasserman. Robust topological inference: Distance to a measure and kernel distance. *J. Mach. Learn. Res.*, 18(1):5845–5884, January 2017.

- [23] Robert J. Adler, Sarit Agami, and Pratyush Pranav. Modeling and replicating statistical topology and evidence for cmb nonhomogeneity. *Proceedings of the National Academy of Sciences*, 114(45):11878–11883, 2017.
- [24] R.J. Adler and S. Agami. Modelling persistence diagrams with planar point processes, and revealing topology with bagplots. *J Appl. and Comput. Topology*, 3:139–183, 2019.
- [25] Adrian Baddeley and Rolf Turner. Practical maximum pseudolikelihood for spatial point patterns. *Australian & New Zealand Journal of Statistics*, 42(3):283–322, 2000.
- [26] Mark Berman and T. Rolf Turner. Approximating point process likelihoods with glim. *Journal of the Royal Statistical Society. Series C (Applied Statistics)*, 41(1):31–38, 1992.
- [27] Atsuyuki Okabe, Barry Boots, Kokichi Sugihara, and Sung Nok Chiu. *Spatial Tessellations: Concepts and Applications of Voronoi Diagrams*. Series in Probability and Statistics. John Wiley and Sons, Inc., 2nd ed. edition, 2000.
- [28] Peter J. Green. Reversible jump markov chain monte carlo computation and bayesian model determination. *Biometrika*, 82(4):711–732, 1995.
- [29] C.J. Geyer and J. Moller. Simulation procedures and likelihood inference for spatial point processes. *Scand. J. Statist*, 21:359–373, 1994.